Chemical Science

ROYAL SOCIETY OF CHEMISTRY

EDGE ARTICLE

View Article Online
View Journal | View Issue

Cite this: *Chem. Sci.*, 2024, **15**, 15448

All publication charges for this article have been paid for by the Royal Society of Chemistry

Received 10th June 2024
Accepted 20th August 2024

DOI: 10.1039/d4sc03796k

rsc.li/chemical-science

Visible light-driven molecular oxygen activation for oxidative amidation of alcohols using lead-free metal halide perovskite†

Vishesh Kumar,[a] Ved Vyas,[a] Deepak Kumar,[a] Ashish Kumar Kushwaha[b] and Arindam Indra *[a]

Herein, we report the modulation of the band structures of halide perovskite Cs_2CuBr_4 by tuning the synthesis methods. The photocatalyst PC-1, synthesized by the hot injection method, has a more negative conduction band minima (CBM) than the photocatalyst PC-2, synthesized at room temperature. As a result, PC-1 can activate molecular O_2 more efficiently to initiate the radical-mediated dehydrogenation of alcohols. The more positive valence band maxima (VBM) of PC-1 also facilitates amine oxidation to the corresponding radical. Further, improved charge separation and transport and a decrement in the photogenerated charge carrier recombination have been detected for PC-1 to enhance photocatalytic activity. PC-1 showed improved yields for a series of structurally diverse amides (highest yield = 98%) by oxidative amidation of alcohols under visible light irradiation.

Introduction

Amides are essential functional groups in natural compounds as well as in diverse industries like polymers, pharmaceuticals, drugs, biomolecules, agrochemicals, *etc.*[1–4] Traditionally, the reaction of amines with carboxylic acid derivatives has been followed to access different amides.[5] Further, Schmidt, Ugi, Staudinger, and Ritter reactions have been applied for amide synthesis.[2,5–9] However, the drawbacks associated with these approaches have prompted the development of safer protocols. Recent advancements include catalytic oxidative amidation, transamination of primary amides using amines, and acylation of amines.[10,11] Among these, one notably eco-friendly method is the catalytic oxidative amidation of benzaldehydes and benzyl alcohols using amines.[1]

In addition, photocatalytic processes using Ru- and Ir-based photocatalysts have been widely explored.[2,12–14] Organo-photocatalysts such as phenazine salts,[15,16] rose Bengal,[17] quinolinium compounds,[16] acridinium salts,[16] *etc.* have also been reported.[16] Although improved activity and selectivity for amides have been achieved with these catalyst systems, the widespread application is often hindered by the requirement of expensive metal and ligand, costly reagents, and poor recycling capacity.

Recently, alternative approaches for the oxidative amidation of aldehydes using visible-light semiconductors have been reported with improved recycling performance. For example, heterogeneous semiconductor catalysts like Ag/g-C_3N_4, Ni/g-C_3N_4, TiO_2, Mn_3O_4, Pd/MIL-101(Fe), Fe_3O_4/PDA/CdS, TzPm-COF, [Ni(dmgH)$_2$]-$CsPbBr_3$, *etc.* have been explored for oxidative amidation of aldehydes with amines.[14,16,18–20] However, these methods often rely on photocatalysts having fewer active sites, fast charge recombination, and limited optical properties.

In contrast, amide bond formation involving the reaction of benzyl alcohol and amine presents an appealing alternative. The efficiency of the dehydrogenative coupling reaction can be improved using alcohols as the substrates instead of aldehydes. Alcohols are largely abundant, less toxic, and less expensive feedstocks, and their direct use makes the process more sustainable.

Milstein group first demonstrated the amidation of alcohols by hydrogen atom transfer (HAT) using ruthenium pincer complex as the catalyst.[21] Later, the HAT process was explored for the amidation of the alcohols using transition metal and noble metal-based catalysts.[22,23] However, these processes suffer from drawbacks like the requirement of high temperature and the use of excessive oxidants and bases. In this context, Yin group explored photocatalytic approach for the amidation of alcohols using Ag_2O/P–C_3N_4.[13]

On the other hand, halide perovskites have emerged as promising photocatalysts for different energy conversion processes[24–26] and organic photoredox reactions because of their unique optoelectronic properties, such as tunable bandgaps, high charge carrier mobility, and low exciton binding energy.[24,27–30] Although Pb-based perovskites, particularly

[a]*Department of Chemistry, Indian Institute of Technology (BHU), Varanasi, UP 221005, India. E-mail: arindam.chy@iitbhu.ac.in; Tel: +919919080675*

[b]*Department of Chemistry, Banaras Hindu University, Varanasi, UP 221005, India*

† Electronic supplementary information (ESI) available: Catalyst synthesis, characterizations, optimization of the catalytic reactions, and ^{1}H NMR and ^{13}C NMR spectra are available. See DOI: https://doi.org/10.1039/d4sc03796k

$CsPbBr_3$, have been extensively studied for photocatalytic energy conversion and organic transformation reactions, the high toxicity of lead and the sensitivity of the perovskites to water limits their further applications.[31] This motivates the search for lead-free perovskites with high photoredox activity.

Previously, Dong *et al.* reported superior photocatalytic activity of Cs_2CuBr_4 compared to $CsPbBr_3$ for photocatalytic CO_2 reduction reaction.[32] Copper, a 3d-metal with unique physicochemical properties, offers multiple valences to optimize the d-band structure. Further, the adjacent Lewis acid (Cu^{2+}) and Lewis base (Br^-) sites in the surface of Cs_2CuBr_4 can generate surface-frustrated Lewis pair sites-which optimize adsorption of the substrate on the catalyst surface.[33–36]

These fascinating properties of Cs_2CuBr_4 have prompted us to explore its photoredox activity for the organic transformation reaction. Further, we have modulated the band structure of Cs_2CuBr_4 by varying the synthesis methods (Scheme 1). The hot injection method produces PC-1 with a smaller size of nanoparticles compared to room temperature method (PC-2). The effect of the size of Cs_2CuBr_4 nanoparticles is found to be pronounced for the bandgap (PC-1: 1.89 eV *vs.* PC-2: 1.64 eV) and band positions ($CBM_{PC\text{-}1}$: −0.80 eV *vs.* $CBM_{PC\text{-}2}$: −0.72 eV and $VBM_{PC\text{-}1}$: 1.09 eV *vs.* $VBM_{PC\text{-}2}$: 0.92 eV). Further, PC-1 showed better charge separation and transport of photogenerated charge carriers compared to PC-2. In addition, the more positive VBM of PC-1 (than PC-2) facilitates the formation of cationic radicals from amines by hole transfer.

The conduction band minima of PC-1 and PC-2 are sufficiently negative (−0.80 V *vs.* NHE) for the reduction of O_2 to $O_2^{\bullet-}$ (−0.33 V *vs.* NHE). Therefore, the electron transfer from the conduction band of Cs_2CuBr_4 to the LUMO of molecular O_2 favors the formation of superoxide radicals. Previously, the activation of molecular O_2 and its interaction with lead halide perovskites has been reported by different groups.[37] These studies have revealed that the molecular O_2 is adsorbed on the surface of perovskite by weak van der Waals forces and the electron transfer from the perovskite to O_2 results in the formation of a strong Pb–O bond.[38] This leads to the structural damage of the perovskite. However, an increase in the photoluminescence life-time and emission quantum yield of perovskite in the presence of O_2 was observed.[39] Therefore, the optoelectronic properties of the perovskite are significantly tuned in the presence of O_2 to facilitate the charge-transfer dynamics.

Although both the photocatalysts (PC-1 and PC-2) can activate molecular O_2 to superoxide radicals, the optimized bandgap, band positions, and the presence of the surface ligands in PC-1 facilitate the O_2 reduction process. As a result, PC-1 achieved high efficiency for the oxidative amidation of alcohols with amines to form structurally diverse amides (highest yield = 98%). Moreover, the catalyst PC-1 can be recycled five times with a minimum loss of initial activity.

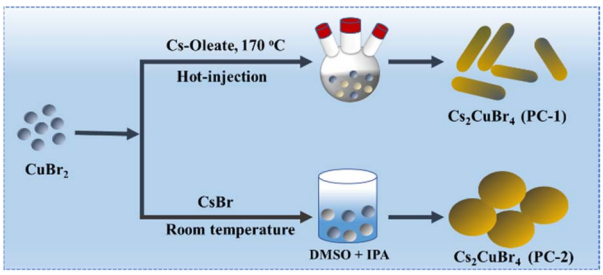

Scheme 1 Schematic representation showing the structural modulation of Cs_2CuBr_4 by two different synthesis methods: (i) hot-injection (PC-1) and (ii) room temperature (PC-2).

Results and discussion

Syntheses and characterizations of the catalysts

Previously, the synthesis of Cs_2CuBr_4 was reported by a room temperature method.[40,41] In this study, we have developed a hot injection method to synthesize Cs_2CuBr_4 nanoparticles (PC-1) with smaller particle size than that of room temperature one (PC-2) (Table S1, ESI†).[27,28] The oleylamine on the surface of PC-1 controls the size and shape of the nanoparticles and prevents their aggregation. The infra-red (IR) spectroscopy detected the vibrations of oleylamine in PC-1 also (Fig. S1†).[42]

The powder X-ray diffraction pattern (PXRD) confirmed the orthorhombic crystal structure of Cs_2CuBr_4 (JCPDS: 71-1462) with space group *Pnma* (Fig. S2†).[32] The PXRD peaks of PC-1 are positively shifted compared to that of PC-2.

The scanning electron microscopy (SEM) detected large particles (>500 nm) with irregular morphology for PC-2 and rod-shaped particles for PC-1 (Fig. 1a and S3†). Transmission electron microscopy (TEM) also revealed the rod-shape morphology of PC-1 with size ranging from 100–200 nm (Fig. 1b).[32,40,41] High-resolution TEM (HRTEM) confirmed the lattice spacing of 0.32 nm, corresponding to the (203) plane of Cs_2CuBr_4 (Fig. 1c). Further, Fast Fourier transformed (FFT) and inverse FFT revealed the (203) plane of Cs_2CuBr_4 (Fig. 1d and d′). The EDX spectrum of PC-1 and PC-2 confirmed the presence of Cs, Cu, and Br (Fig. S4 and S6†). The EDX elemental mapping also detected a uniform distribution of the elements Cs, Cu, and Br (Fig. S5 and S7†).

The variation in the synthetic method of Cs_2CuBr_4 not only shifts the PXRD peaks, it also tunes the electronic structure of the elements as detected by X-ray photoelectron spectroscopy (XPS). The Cs 3d XPS was deconvoluted into two peaks for Cs $3d_{5/2}$ and Cs $3d_{3/2}$ (Fig. 1e). A positive shift of the Cs $3d_{5/2}$ peak by 0.49 eV was detected for PC-1, indicating a significant variation in the electron density around Cs.

Further, the Cu 2p XP spectra were fitted for Cu $2p_{3/2}$ and Cu $2p_{1/2}$ peaks (Fig. 1f).[32,40,41] Similar to Cs, the positive shift of the $2p_{3/2}$ peak by 0.62 eV was detected for Cu. The Cu^{2+}/Cu^+ ratio of PC-1 and PC-2 was calculated to be 2.65 and 1.31, respectively. PC-1 has a higher Cu^{2+}/Cu^+ ratio compared to PC-2. The modulation of the electronic structure was also confirmed from the Cu $2p_{3/2}$-$2p_{1/2}$ spin–orbit coupling values for PC-1 (21.69 eV) and PC-2 (22.24 eV) respectively. The higher Cu^{2+}/Cu^+ ratio in PC-1 improved the Lewis acid character to improve the adsorption of the substrates.

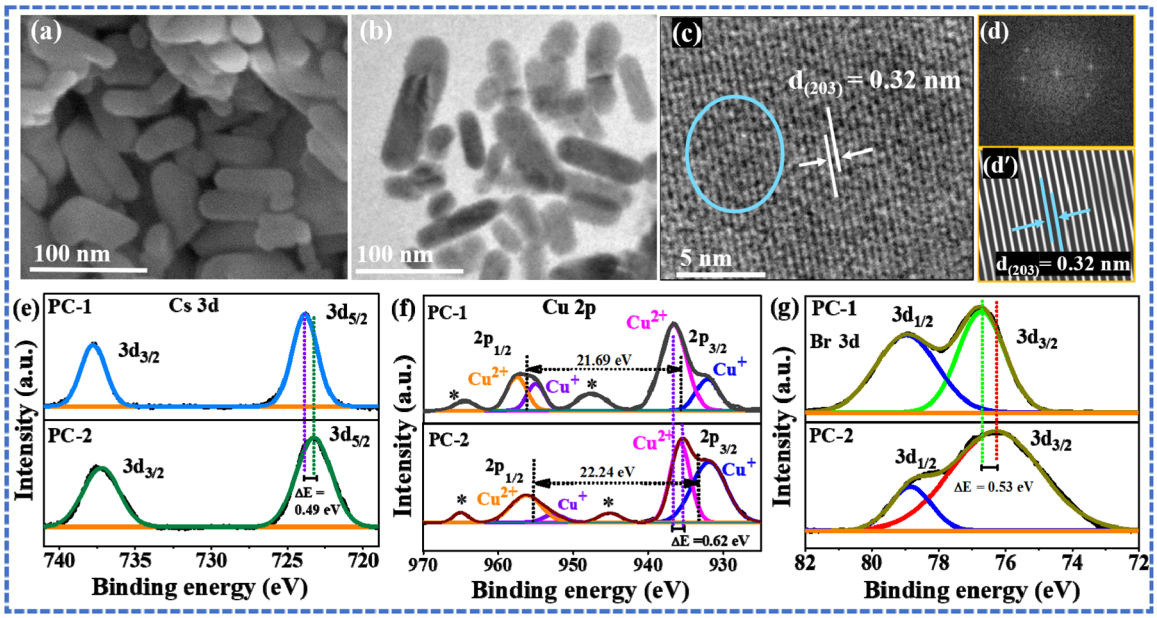

Fig. 1 (a) SEM image showing the rod shape morphology of PC-1; (b) TEM image of PC-1, showing nanorod morphology. (c) High-resolution TEM image showing the lattice spacing corresponding to (203) plane of Cs_2CuBr_4. (d) Fast Fourier transformed (FFT) and (d′) inverse FFT corresponding to the selected circle area of (c). Comparison of the XPS of PC-1 and PC-2 showing in figure (e) Cs 3d, (f) Cu 2p, (g) Br 3d. The XPS peaks of Cs, Cu, and Br showed a positive shift in PC-1 compared to PC-2 because of the structural modulation.

Br 3d peak was also shifted to higher binding energy (0.53 eV) for PC-1 than PC-2 (Fig. 1g). The electronic structure modulation leads to a significant variation in the photocatalytic activity for oxidative amidation of alcohols with amines (see later).

Optoelectronic properties of the photocatalysts

The UV-visible diffuse reflectance spectroscopy (DRS) revealed the absorption properties and bandgap (Fig. 2a).[32,43] From the Tauc plots, the bandgaps of PC-1 and PC-2 were calculated to be 1.89 eV and 1.64 eV, respectively (Fig. 2a, inset). The light absorption of PC-1 extends from the visible to the near-infra-red region (Fig. 2a).[32,43,44]

The Mott–Schottky plots displayed positive slopes within the frequency range of 0.5–1.5 kHz, indicating the n-type nature of both PC-1 and PC-2 (Fig. 2b and S8†).[32,44,45] The Fermi level energy (E_f) of PC-1 and PC-2 was found to be −0.70 and −0.62 eV. The CBM for n-type semiconductors is 0.1 or 0.2 eV higher than the flat band potential (see details in ESI†).[46] Therefore, the CBMs for PC-1 and PC-2 were determined to be −0.80 and −0.72 V *vs.* the normal hydrogen electrode (NHE), respectively (Fig. 2c). The VBMs of PC-1 and PC-2 were calculated to be 1.09 and 0.92 eV *vs.* NHE, respectively.

The electronic band structure plays a pivotal role in regulating photocatalytic activity. PC-1 exhibited a wider band gap (1.89 eV) than that of PC-2 (1.64 eV). The more negative CBM of PC-1 (than PC-2) also facilitates the activation of molecular oxygen-forming superoxide radicals to initiate the C–N coupling reaction for the amide formation (see later).

Further, cyclic voltammetry (CV) measurements were carried out to understand the electronic structure of the catalysts. As the redox peak positions in the CV are not prominent, we have carried out differential pulse voltammetry (DPV) in the dark and light (Fig. S9†). Interestingly, the peak positions for PC-1 in the dark and light did not show any significant variation (Fig. S9†). However, the highly negative reduction peaks in PC-1 compared to PC-2 helps in the facile activation of molecular oxygen during the photocatalytic process.

Photoluminescence (PL) spectra showed an emission peak at 460 nm for both the catalysts and the intensity of the emission peak was found to be significantly lower for PC-1 (Fig. 2d).[47–50] The photocurrent measurements confirmed better charge separation and transport in PC-1 compared to PC-2 (Fig. 2e).[51–54] The charge transport properties of the catalysts were further investigated through electrochemical impedance spectroscopy (EIS) studies and in the presence of light, low charge transfer resistance was detected for PC-1 (Fig. 2f).[32,40,41,43–45] These results indicate that smaller particle size of PC-1 results in a better charge separation and transport than that in PC-2 to improve the photocatalytic oxygen activation.

Optimization of reaction conditions for the amidation of alcohols

The photocatalytic amidation of alcohols (**1**) and different amines (**2**) in the presence of PC-1 and PC-2 produced amides (**3**) under visible light irradiation. The optimization process for photocatalytic amidation was conducted by the reaction of 4-nitrobenzyl alcohol and pyrrolidine. Initially, the photocatalytic activity of PC-1 and PC-2 was evaluated (Table 1) and a better photocatalytic activity of PC-1 was observed to produce 4-nitrophenyl(pyrrolidine-1-yl)methanone with 97% yield (entry 1, Table 1). Under similar reaction conditions, the yield for the

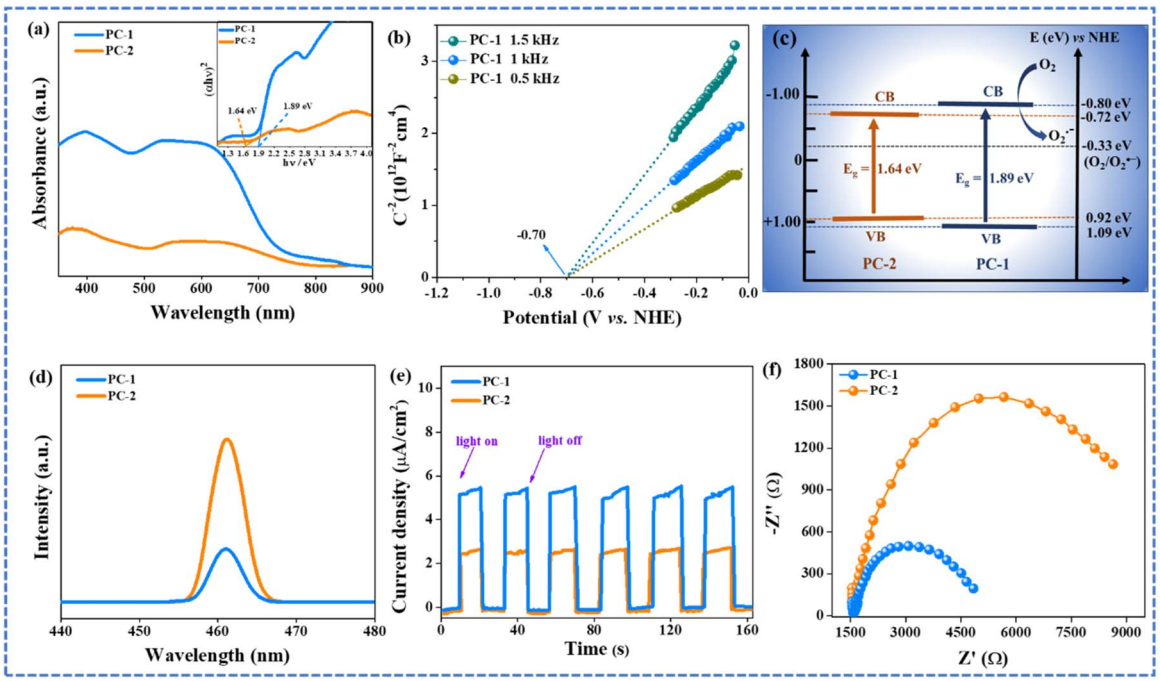

Fig. 2 (a) The UV-vis. diffuse reflectance spectra of PC-1 and PC-2, inset showing the corresponding Tauc plot, demonstrating a significant change in the band gap for PC-1 and PC-2. (b) Mott–Schottky plot of PC-1. (c) The conduction band minima and valence band maxima for PC-1 and PC-2, derived from Tauc plot and Mott–Schottky studies. (d) Photoluminescence spectra of PC-1 and PC-2 showing the reduced PL intensity in PC-1. (e) Photocurrent measurements of PC-1 and PC-2 under light/dark conditions showing better charge separation in PC-1. (f) Electrochemical impedance spectroscopic studies of PC-1 and PC-2 in light reveal the low charge transfer resistance for PC-1.

Table 1 Comparison of the photocatalytic activities of PC-1 and PC-2 for the amidation of alcohols in the presence of light[a]

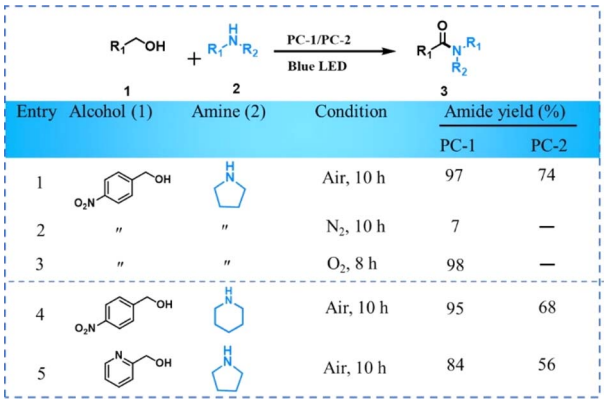

Entry	Alcohol (1)	Amine (2)	Condition	Amide yield (%)	
				PC-1	PC-2
1			Air, 10 h	97	74
2	〃	〃	N_2, 10 h	7	—
3	〃	〃	O_2, 8 h	98	—
4			Air, 10 h	95	68
5			Air, 10 h	84	56

[a] Reaction conditions: alcohol (0.5 mmol), amine (1.0 mmol), photocatalyst (10 mg), THF (3 mL), 15 W blue LED, temperature: 35 ± 2 °C, time: 10 h. In all the cases, isolated yield of the product was reported and ^{1}H and ^{13}C NMR was used to characterize the products.

same reaction was found to be 74% with PC-2 and even after 15 h of reaction, the yield was only increased 94%. To further confirm the improved photocatalytic activity of PC-1, we have carried out the reactions of 4-nitrobenzyl alcohol with piperidine and 2-pyridine methanol with pyrrolidine (Table 1). In all the cases, significantly higher yields for the amides have been detected for PC-1 than PC-2.

The role of molecular oxygen is crucial for the amidation reaction and the formation of amide is not detected in the presence of N_2. The molecular O_2 (in air) is reduced to superoxide radicals by the transfer of photogenerated electrons from the CB of Cs_2CuBr_4 (Fig. 2c). Further, superoxide radicals initiate the dehydrogenation of benzyl alcohol. Therefore, in the absence of O_2, the amide formation was not observed. The reaction was found to be faster in pure O_2 compared to air (Table 1). The yield of 4-nitrophenyl(pyrrolidine-1-yl)methanone was extremely low (4%) in the dark and no reaction took place in the absence of catalyst. Among different solvents, the best result was obtained in tetrahydrofuran (THF) (Table S2†).

Substrate scope for the amide synthesis

The amide bond formation strategy using derivatives of alcohols and secondary amines, demonstrated a broad substrate scope and tolerance to diverse functional groups, achieving excellent yields. The substrate scope of different alcohols was studied under the optimal conditions reacting with pyrrolidine to form a series of amides (Table 2, **3a–k**). Notably, the substituents in the benzyl alcohols exerted a significant influence on the amide yield. Substrates with the electron-donating group in the phenyl ring of benzyl alcohols (4-methylbenzyl alcohol and 4-methoxybenzyl alcohol) showed slightly low yields (Table 2, **3b** and **3c**). The steric crowding in the phenyl ring of 3,4,5-trimethoxybenzyl alcohol also decreased the yield of the amide (Table 2, **3d**).

Table 2 The substrate scope of different alcohols and amines for amide bond formation[a]

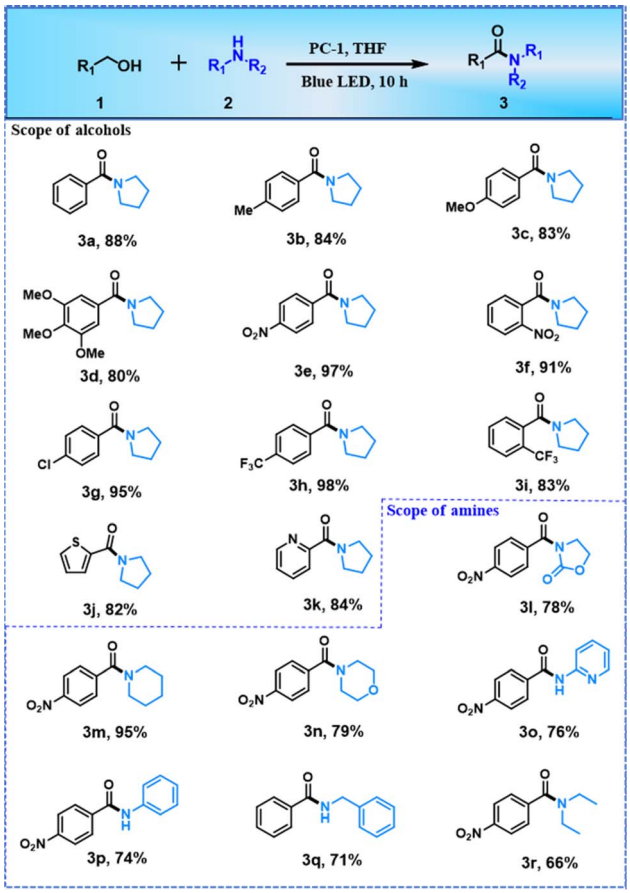

[a] Reaction conditions: alcohol (0.5 mmol), amine (1.0 mmol), PC-1 (10 mg), THF (3 mL), 15 W blue LED, air, temperature: 35 ± 2 °C, time: 10 h. In all the cases, isolated yield of the product was reported and the products were characterized by ^{1}H and ^{13}C NMR spectroscopy (Table S3).

In contrast, the electron-withdrawing group at the *para*-position of benzyl alcohol produced slightly higher yield of amides (Table 2, **3e** and **3h**). Even, 4-chlorobenzylalcohol produced a good yield of amide (95%) under similar reaction conditions (Table 2, **3g**). The trifluoromethyl group at *para*-position of the phenyl ring also produced a high yield of amide (Table 2, **3h**).

The reaction of 2-nitrobenzyl alcohol with pyrrolidine produced **3f**, a well-known insect repellent, with 91% yield.[55] However, the electron-withdrawing group ($-NO_2$ and $-CF_3$) at the *ortho*-position of benzyl alcohol produced a slightly lower yield of amide compared to that in the *para*-position, most probably due to the steric crowding at the *ortho*-position (Table 2, **3f**, and **3i**).

The electron-donating or withdrawing properties of the substituents at different positions (*ortho*-, *meta*-, or *para*-) of the phenyl ring of benzyl alcohol may have a complicated impact on the conversion efficiency and product yield. For example, the electron-donating group at the *para*-position of benzyl alcohol can facilitate the C_α–H abstraction by $O_2^{\bullet-}$ but the electron-withdrawing group can stabilize the intermediate benzylic radical for a facile C–N coupling.

The photocatalytic amidation was also found to be effective for the heterocyclic alcohols to produce more than 82% yield of the amides. However, the amide yields are low for heterocyclic alcohols compared to benzyl alcohol (Table 2, **3j** and **3k**).

The variation of the amine also affected the amide yields. The amines like 2-oxazolidine or morpholine, when reacted with 4-nitro benzyl alcohol, a significant decrease in the amide yield was observed compared to pyrrolidine (Table 2, **3e** *vs.* **3l** and **3n**) while piperidine produced similar yield of amide (Table 2, **3m**).

Interestingly, heterocyclic amine (2-aminopyridine) yielded 76% amide when reacted with 4-nitrobenzyl alcohol (Table 2, **3o**). However, aniline reduced the yield of amide (Table 2, **3p**). Further, benzylamine produced 71% yield of amide reacting with benzyl alcohol (Table 2, **3q**). However, amide yield was significantly reduced when 4-nitrobenzyl alcohol was reacted with open-chain aliphatic amine (diethyl amine) (Table 2, **3r**).

The above results showed that the yields of amides for aliphatic cyclic amines are higher than that for aliphatic acyclic amines, aromatic primary amines, and hetero-aromatic amines. The poor nucleophilic nature of aromatic primary amine and hetero-aromatic amine and the steric crowding in aliphatic acyclic amine reduced the amide yield.[7,19] The presence of strong electronegative oxygen in the ring of aliphatic cyclic amine (morpholine and 2-oxazolidine) also reduced the nucleophilic character of it and hence a low product yield was obtained.[55] The catalyst stability was evaluated by recycling 5 cycles with a minimum loss of photocatalytic activity (Fig. S10†). After 5 cycles of oxidative amidation of 4-nitrobenzyl alcohol, no significant change in the UV-visible-DRS spectrum of PC-1 was observed (Fig. S11†). The IR spectroscopy also detected the presence of the surface oleylamine in PC-1 after the first catalytic cycle (Fig. S12a†).

The effect of surface ligand on the photocatalytic reaction is complex. The surface ligand reduces the non-radiative recombination process and improves the system's photoluminescence property, and hence can improve the photocatalytic activity. On the other hand, the ligand can also passivate the catalyst surface, inhibiting the substrate binding.[56,57] As the surface ligand plays an important role in charge separation and transport of the photocatalyst, we have checked the activity of PC-1 after the complete removal of the ligand oleylamine from the catalyst surface (see in the experimental part, ESI) (Fig. S12b).† The removal of surface ligand from PC-1 leads to a slight decrease in the yield (87%) of the amide.

Mechanism of photocatalytic reaction

Based on the results obtained from the controlled experiments and the detected reaction intermediates, the mechanism of the photocatalytic amidation of alcohols has been explained. The visible light irradiation results in exciton generation, subsequent transport, and separation, followed by the transfer of the photogenerated electrons from the CB of Cs_2CuBr_4 to molecular oxygen.

The process of C–N bond formation is governed by two steps: (i) the single electron reduction of O_2 to $O_2^{\bullet-}$ radicals and (ii) oxidation of the amine to the corresponding cationic radicals (**2a***) by the holes (h^+) in the valence band. As PC-1 has a more negative CBM ($E_{CB} = -0.80$ V *vs.* NHE, pH = 7) than PC-2, the single electron reduction of O_2 to $O_2^{\bullet-}$ ($O_2 + e^- \rightarrow O_2^{\bullet-}$, $E^o = -0.33$ V *vs.* NHE, pH = 7) is favored for the former.[19] Further $O_2^{\bullet-}$ initiates the dehydrogenation of 4-nitrobenzyl alcohol and form benzyl radical (**1e***) and $^{\bullet}$OOH. The bond dissociation energy of C_α–H bond (79.3 kcal mol^{-1}) in benzyl alcohol is lower than that of the O–H bond (99.0 kcal mol^{-1}).[58] Therefore, the photo-generated $O_2^{\bullet-}$ radicals abstract the hydrogen from C_α–H bond.[59] In the next step, the radical coupling of **1e*** and **2e*** forms an intermediate (**I**$^{\#}$) species. The $^{\bullet}$OOH radicals further abstract proton from **I**$^{\#}$ to form **A*** and hydrogen peroxide. Further reaction of $O_2^{\bullet-}$ with **A*** forms final product **3e** and H_2O_2 (Scheme 2).

In contrast to the previous reports, we are not able to detect the formation of 4-nitrobenzaldehyde by the oxidation of 4-nitrobenzyl alcohol in the presence of pyrrolidine. However, in the absence of amine, 4-nitrobenzyl alcohol is slowly converted into the corresponding aldehyde (Fig. S13†). Further, we have performed the reaction of 4-nitrobenzaldehyde with pyrrolidine and the rate of the reaction was found to be slower than that of 4-nitrobenzyl alcohol and pyrrolidine. The reaction rate for the oxidation of 4-nitrobenzyl alcohol (without pyrrolidine) to 4-nitrobenzaldehyde was found to be slower than the C–N bond formation but faster than the reaction of 4-nitrobenzaldehyde with pyrrolidine (Fig. S13†). The above experiments showed that the photocatalytic reaction proceeds through the direct coupling of 4-nitrobenzyl alcohol and pyrrolidine instead of the benzaldehyde route. These studies confirmed the radical coupling of **1e*** and **2e*** to form **I**$^{\#}$ compared to the oxidation of **1e** to 4-nitrobenzaldehyde.

A series of quenching experiments were carried out to understand the involvement of the electrons from the CB, holes from the VB, and $O_2^{\bullet-}$ radicals (Fig. S14†). The addition of $AgNO_3$ and triethylamine as the electron and hole scavenger resulted in a significant drop in the yield of 3e to 12% and 15%, respectively.[60] In addition, when 4-benzoquinone (BQ) was used as a superoxide radical ($O_2^{\bullet-}$) scavenger, the yield of amide decreased to 21% (Fig. S14†).[58,61,62]

The involvement of the radical mechanism was also proved by radical trapping reaction. In the presence of TEMPO (2,2,6,6-Tetramethylpiperidine-1-oxyl), the yield of **3e** was reduced to 18% (Fig. S15†). Further, we are able to detect TEMPO-**1e*** and TEMPO-**2e*** adducts by mass spectrometry (Fig. S15†). The production of $O_2^{\bullet-}$ was detected by *p*-nitro-blue tetrazolium chloride (NBT) test (Fig. S16†).[63] The UV-visible spectroscopy confirmed (NBT test) that PC-1 produced more $O_2^{\bullet-}$ compared to PC-2.[64]

The formation of H_2O_2 was also detected by using *o*-tolidine as an indicator (Fig. S17†).[65–67] Therefore, it is clear that PC-1 is more effective in the activation of molecular oxygen compared to PC-2 (Fig. S16 and S17†). Overall, the above study revealed that PC-1 nanoparticles showed improved photocatalytic activity compared to that of PC-2.

According to previous reports, copper(II) sites in the catalyst facilitate the electron transfer process and stabilize the reactive intermediates formed during the coupling reaction, thereby influencing the reaction kinetics and selectivity of the products.[68] Cu(I) sites typically initiate C–N coupling reactions.[69,70] Therefore, the presence of both Cu(II) and Cu(I) sites in PC-1 is beneficial for the selective C–N coupling of alcohol and amine.

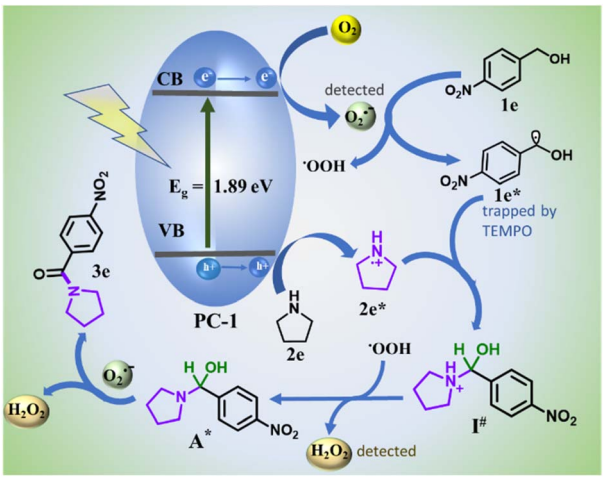

Scheme 2 The proposed mechanism for photocatalytic oxidative amidation of alcohol is based on the detected intermediates.

Conclusions

In summary, we effectively utilized lead-free halide perovskite Cs_2CuBr_4 (PC-1 and PC-2) with different electronic properties and particle size for the photocatalytic amidation of alcohols. The structural differences in the two photocatalysts led to different band structures with more negative CBM and more positive VBM for PC-1 than PC-2. The favorable band positions in PC-1 facilitated photocatalytic O_2 reduction to form superoxide radicals, which helps in the C–N coupling reaction.

Data availability

All the data related to the above-mentioned manuscript are available in the ESI.†

Author contributions

V. K. involved in the synthesis of the catalysts, their characterization, photocatalytic studies, data interpretation, and manuscript writing. V. V. involved in product separation (column chromatography) and NMR. D. K. and A. K. K. carried out (photo)electrochemical characterization and data interpretation. The project design, conceptualization, supervision, data interpretation, manuscript writing, and editing were performed by A. I.

Conflicts of interest

There are no conflicts to declare.

Acknowledgements

A. I. would like to thank DST-SERB, India for the core research grant (Grant no.: CRG/2023/002395). V. K. is thankful to CSIR [09/1217/(0084)/2020-EMR-II] for providing the senior research fellowship.

References

1 S. Das, S. Mondal, S. P. Midya, S. Mondal, E. Ghosh and P. Ghosh, *J. Org. Chem.*, 2023, **88**, 14847–14859.
2 S. Gaspa, A. Farina, M. Tilocca, A. Porcheddu, L. Pisano, M. Carraro, U. Azzena and L. De Luca, *J. Org. Chem.*, 2020, **85**, 11679–11687.
3 V. Vyas, V. Kumar and A. Indra, *Chem. Commun.*, 2024, **60**, 2544–2547.
4 B. Goel, V. Vyas, N. Tripathi, A. Kumar Singh, P. W. Menezes, A. Indra and S. K. Jain, *ChemCatChem*, 2024, **12**, 5743–5749.
5 J. Kweon, B. Park, D. Kim and S. Chang, *Nat. Commun.*, 2024, **15**, 3788.
6 X. Chen, Z. Lian and S. Kramer, *Angew. Chem. Int. Ed.*, 2023, **135**, e202217638.
7 H. Ghafuri, M. G. Gorab and H. Dogari, *Sci. Rep.*, 2022, **12**, 2331.
8 B. Lu, W. L. Xiao and J. R. Chen, *Molecules*, 2022, **27**, 517.
9 J. Liu, C. Zhang, Z. Zhang, X. Wen, X. Dou, J. Wei, X. Qiu, S. Song and N. Jiao, *Science*, 2020, **367**, 281–285.
10 A. Hassan Tolba, M. Krupička, J. Chudoba and R. Cibulka, *Org. Lett.*, 2021, **23**, 6825–6830.
11 X. Zhu, Y. Lin, J. San Martin, Y. Sun, D. Zhu and Y. Yan, *Nat. Commun.*, 2019, **10**, 4279.
12 N. J. Oldenhuis, V. M. Dong and Z. Guan, *Tetrahedron*, 2014, **70**, 4213–4218.
13 L. Deng, L. Chen, L. Zhu, Y. Li, J. Ou-Yang, S. Wu, P. Chen, S. Shen, J. Guo, Y. Zhou, C. T. Au and S. F. Yin, *Chem. Eng. Sci.*, 2022, **261**, 117960.
14 A. Rashidizadeh, H. Ghafuri, N. Goodarzi and N. Azizi, *Solid State Sci.*, 2020, **109**, 106427.
15 D. Leow, *Org. Lett.*, 2014, **16**, 5812–5815.
16 Z. Akrami and M. Hosseini-Sarvari, *Eur. J. Org. Chem.*, 2022, e202200429.
17 F. K. C. Leung, J. F. Cui, T. W. Hui, K. K. Y. Kung and M. K. Wong, *Asian J. Org. Chem.*, 2015, **4**, 533–536.
18 Y. Long, J. Wen, L. Zhu, L. Zeng, M. Lu and L. Deng, *J. Photochem. Photobiol., A*, 2024, **453**, 115612.
19 A. Dey, S. Chakraborty, A. Singh, F. A. Rahimi, S. Biswas, T. Mandal and T. K. Maji, *Angew. Chem., Int. Ed.*, 2024, e202403093.
20 V. Kumar, S. K. Patel, V. Vyas, D. Kumar, E. S. S. Iyer and A. Indra, *Chem. Sci.*, 2024, **15**, 13218–13226.
21 J. P. Stephenson, J. E. Patterson, W. Huang, D. D. Dlott, J. G. Fujimoto, E. P. Ippen, P. B. Davies, T. H. Ong, R. N. Ward, M. Hara, H. Sasabe, K. Wolfgang, C. Kodama, H. Sumida, H. Nozoye, S. Lagutchev, D. G. Cahill, P. V. Braun, R. Segalman, A. Majumdar, M. T. Seidel, H. Zewail and F. Seitz, *Science*, 2007, **317**, 790–792.
22 A. Kumar, N. A. Espinosa-Jalapa, G. Leitus, Y. Diskin-Posner, L. Avram and D. Milstein, *Angew. Chem. Int. Ed.*, 2017, **56**, 14992–14996.
23 V. Vyas, P. Maurya and A. Indra, *Chem. Sci.*, 2023, **14**, 12339–12344.
24 H. Huang, B. Pradhan, J. Hofkens, M. B. J. Roeffaers and J. A. Steele, *ACS Energy Lett.*, 2020, **5**, 1107–1123.
25 P. Zhang, Y. Tong, Y. Liu, J. J. M. Vequizo, H. Sun, C. Yang, A. Yamakata, F. Fan, W. Lin, X. Wang and W. Choi, *Angew. Chem., Int. Ed.*, 2020, **59**, 16209–16217.
26 Y. Dai, C. Poidevin, C. Ochoa-Hernández, A. A. Auer and H. Tüysüz, *Angew. Chem., Int. Ed.*, 2020, **132**, 5837–5845.
27 Y. Li, Y. Gao, Z. Deng, Y. Cao, T. Wang, Y. Wang, C. Zhang, M. Yuan and W. Xie, *Nat. Commun.*, 2023, **14**, 4673.
28 K. Mishra, D. Guyon, J. San Martin and Y. Yan, *J. Am. Chem. Soc.*, 2023, **145**, 17242–17252.
29 Y. Li, T. Wang, Y. Wang, Z. Deng, L. Zhang, A. Zhu, Y. Huang, C. Zhang, M. Yuan and W. Xie, *ACS Catal.*, 2022, **12**, 5903–5910.
30 I. Rosa-Pardo, D. Zhu, A. Cortés-Villena, M. Prato, L. De Trizio, L. Manna, R. E. Galian and J. Pérez-Prieto, *ACS Energy Lett.*, 2023, **8**, 2789–2798.
31 H. Jiang, M. Liu, X. Lian, M. Zhu and F. Zhang, *Angew. Chem., Int. Ed.*, 2024, **136**, e202318850.
32 J. Sheng, Y. He, M. Huang, C. Yuan, S. Wang and F. Dong, *ACS Catal.*, 2022, **12**, 2915–2926.
33 T. Yan, N. Li, L. Wang, W. Ran, P. N. Duchesne, L. Wan, N. T. Nguyen, L. Wang, M. Xia and G. A. Ozin, *Nat. Commun.*, 2020, **11**, 6095.
34 S. Zhang, Z. Q. Huang, Y. Ma, W. Gao, J. Li, F. Cao, L. Li, C. R. Chang and Y. Qu, *Nat. Commun.*, 2017, **8**, 15266.
35 T. Cai, W. Shi, S. Hwang, K. Kobbekaduwa, Y. Nagaoka, H. Yang, K. Hills-Kimball, H. Zhu, J. Wang, Z. Wang, Y. Liu, D. Su, J. Gao and O. Chen, *J. Am. Chem. Soc.*, 2020, **142**, 11927–11936.
36 P. Cheng, L. Sun, L. Feng, S. Yang, Y. Yang, D. Zheng, Y. Zhao, Y. Sang, R. Zhang, D. Wei, W. Deng and K. Han, *Angew. Chem., Int. Ed.*, 2019, **58**, 16087–16091.
37 J. He, W. H. Fang, R. Long and O. V. Prezhdo, *J. Am. Chem. Soc.*, 2020, **142**, 14664–14673.
38 L. Qiao, W. H. Fang, O. V. Prezhdo and R. Long, *J. Am. Chem. Soc.*, 2022, **144**, 5543–5551.
39 T. Wang, Y. Li, X. Yang, Y. Hu, X. Du, M. Zhang, Z. Huang, S. Liu, Y. Wang and W. Xie, *Angew. Chem., Int. Ed.*, 2024, e202409656.
40 Z. Zhang, D. Li, H. Hu, Y. Chu and J. Xu, *Inorg. Chem.*, 2023, **62**, 9240–9248.
41 Z. Zhang, D. Li, Y. Chu, L. Chang and J. Xu, *J. Phys. Chem. Lett.*, 2023, **14**, 5249–5259.
42 R. Grisorio, F. Fasulo, A. B. Muñoz-García, M. Pavone, D. Conelli, E. Fanizza, M. Striccoli, I. Allegretta, R. Terzano, N. Margiotta, P. Vivo and G. P. Suranna, *Nano Lett.*, 2022, **22**, 4437–4444.

43 J. Qian, H. Hu, Y. Liang and Z. Zhang, *Appl. Surf. Sci.*, 2024, **648**, 159084.
44 Z. Zhang, X. Wang, J. Qian and J. Xu, *J. Energy Chem.*, 2024, **92**, 521–533.
45 H. Tang, X. Wang, C. Yao and Z. Zhang, *Sep. Purif. Technol.*, 2024, **338**, 126544.
46 A. Hankin, F. E. Bedoya-Lora, J. C. Alexander, A. Regoutz and G. H. Kelsall, *J. Mater. Chem. A*, 2019, **7**, 26162–26176.
47 Y. Wang, A. Vogel, M. Sachs, R. S. Sprick, L. Wilbraham, S. J. A. Moniz, R. Godin, M. A. Zwijnenburg, J. R. Durrant, A. I. Cooper and J. Tang, *Nat. Energy*, 2019, **4**, 746–760.
48 Y. T. Xiong, W. X. Liu, L. Tian, P. L. Qin, X. B. Chen, L. Ma, Q. B. Liu, S. J. Ding and Q. Q. Wang, *Adv. Funct. Mater.*, 2024, 2407819.
49 Y. Wang, R. Godin, J. R. Durrant and J. Tang, *Angew. Chem., Int. Ed.*, 2021, **60**, 20811–20816.
50 A. Indra, R. Beltrán-Suito, M. Müller, R. P. Sivasankaran, M. Schwarze, A. Acharjya, B. Pradhan, J. Hofkens, A. Brückner, A. Thomas, P. W. Menezes and M. Driess, *ChemSusChem*, 2021, **14**, 306–312.
51 J. Yang, A. Acharjya, M. Y. Ye, J. Rabeah, S. Li, Z. Kochovski, S. Youk, J. Roeser, J. Grüneberg, C. Penschke, M. Schwarze, T. Wang, Y. Lu, R. Krol, M. Oschatz, R. Schomäcker, P. Saalfrank and A. Thomas, *Angew. Chem., Int. Ed.*, 2021, **60**, 19797–19803.
52 A. Indra, A. Acharjya, P. W. Menezes, C. Merschjann, D. Hollmann, M. Schwarze, M. Aktas, A. Friedrich, S. Lochbrunner, A. Thomas and M. Driess, *Angew. Chem., Int. Ed.*, 2017, **56**, 1653–1657.
53 J. Zhang, W. Ling, A. Li, J. Ma, M. Hong and R. Sun, *Adv. Funct. Mater.*, 2024, e2405420.
54 X. Wang, B. Liu, S. Ma, Y. Zhang, L. Wang, G. Zhu, W. Huang and S. Wang, *Nat. Commun.*, 2024, **15**, 2600.
55 M. Roy, B. Mishra, S. Maji, A. Sinha, S. Dutta, S. Mondal, A. Banerjee, P. Pachfule and D. Adhikari, *Angew. Chem., Int. Ed.*, 2024, e202410300.
56 M. Y. Qi, Y. H. Li, M. Anpo, Z. R. Tang and Y. J. Xu, *ACS Catal.*, 2020, **10**, 14327–14335.
57 H. Wang, W. Lu, P. Xu, J. Luo, K. Yao, J. Zhang, X. Wei, S. Peng, H. Cheng, H. Hu and K. Sun, *ACS Sustain. Chem. Eng.*, 2023, **11**, 5963–5972.
58 Q. Fan, D. Liu, Z. Xie, Z. Le, H. Zhu and X. Song, *J. Org. Chem.*, 2023, **88**, 14559–14570.
59 M. Xiao, M. Hao, M. Lyu, E. G. Moore, C. Zhang, B. Luo, J. Hou, J. Lipton-Duffin and L. Wang, *Adv. Funct. Mater.*, 2019, **29**, 1905683.
60 K. Michalec, B. Mozgawa, A. Kusior, P. Pietrzyk, Z. Sojka and M. Radecka, *J. Phys. Chem. C*, 2024, **128**, 5011–5029.
61 Q. Fan, H. Zhang, D. Liu, C. Yan, H. Zhu, Z. Xie and Z. Le, *J. Org. Chem.*, 2023, **88**, 7391–7400.
62 I. Rosa-Pardo, C. Casadevall, L. Schmidt, M. Claros, R. E. Galian, J. Lloret-Fillol and J. Pérez-Prieto, *Chem. Commun.*, 2020, **56**, 5026–5029.
63 Y. Deng, W. Liu, R. Xu, R. Gao, N. Huang, Y. Zheng, Y. Huang, H. Li, X. Y. Kong and L. Ye, *Angew. Chem., Int. Ed.*, 2024, e202319216.
64 J. Luo, X. Wei, Y. Qiao, C. Wu, L. Li, L. Chen and J. Shi, *Adv. Mater.*, 2023, **35**, 2210110.
65 A. K. Singh, K. Bijalwan, N. Kaushal, A. Kumari, A. Saha and A. Indra, *ACS Appl. Nano Mater.*, 2023, **6**, 8036–8045.
66 A. K. Singh, D. Hollmann, M. Schwarze, C. Panda, B. Singh, P. W. Menezes and A. Indra, *Adv. Sustainable Syst.*, 2021, **5**, 2000288.
67 O. C. Compton and F. E. Osterloh, *J. Phys. Chem. C*, 2009, **113**, 479–485.
68 E. S. Jang, C. L. Mcmullin, M. Käß, K. Meyer, T. R. Cundari and T. H. Warren, *J. Am. Chem. Soc.*, 2014, **136**, 10930–10940.
69 W. P. Carson, A. V. Tsymbal, R. W. Pipal, G. A. Edwards, J. R. Martinelli, A. Cabré and D. W. C. MacMillan, *J. Am. Chem. Soc.*, 2024, **146**, 15681–15687.
70 E. Boess, C. Schmitz and M. Klussmann, *J. Am. Chem. Soc.*, 2012, **134**, 5317–5325.